The effect of magnetic coupling along the magnetic axis on slow magnetic relaxation in Dy^{III} complexes with D_{5h} configuration based on an aggregation-induced-emission-active ligand

Min-Xia Yao*[a], Yu-Qi Gao[a], Zhong-Wu An[a] and Dong-Mei Zhu*[b]

[a]*School of Chemistry & Molecular Engineering, Nanjing Tech University, Nanjing, 211816, P. R. China.*

[b]*Jiangsu Key Lab for NSLSCS, School of Physical Science and Technology, Nanjing Normal University, Nanjing 210023, P. R. China.*

Table S1 Summary of crystallographic data for all complexes.

complexes	**1**	**2**	**3**
molecular formula	$C_{94}H_{110}Cl_2Dy_2N_8O_8P_2$	$C_{102}H_{112}Cl_2Dy_2N_6O_6P_2$	$C_{98}H_{102}Cl_2Dy_2N_{12}O_{12}P_2$
formular weight	1933.70	1975.81	2097.75
crystal system	Triclinic	Triclinic	Orthorhombic
space group	*P*-1	*P*-1	*P*bca
a, Å	11.7971(5)	11.1140(6)	24.0573(8)
b, Å	13.9098(7)	15.1554(9)	36.8217(13)
c, Å	16.1086(7)	15.9704(9)	10.7953(4)
a, deg	65.090(2)°	64.553(2)	90
β, deg	82.000(2)°	85.699(2)	90
γ, deg	74.102(2)°	77.051(2)	90
V, Å^3	2304.88(19)	2366.6(2)	9562.8(6)
Z	1	1	4
ρ_{calcd},g cm^{-3}	1.393	1.386	1.457
T / K	193	193	193
μ, mm^{-1}	1.759	1.713	1.706
θ, deg	2.121 to 26.000	2.153 to 26.000	2.022 to 27.506
F(000)	986	1010	4264
index ranges	−14 ≤ h ≤ 14 −17 ≤ k ≤17 −19≤ l ≤ 19	−13 ≤ h ≤ 13 −18 ≤ k ≤18 −19≤ l ≤ 18	−31 ≤ h ≤ 22 −47 ≤ k ≤47 −14≤ l ≤ 12
data/restraints/parameters	9052/1306/608	9128/1444/524	10952/32/587

* To whom correspondence should be addressed. Email: yaomx@njtech.edu.cn; Fax: +86-25-58139528.
* To whom correspondence should be addressed. Email: 221001007@njnu.edu.cn.

GOF (F^2)	1.086	1.116	1.087
$R_1{}^a$,$wR_2{}^b$ (I>2σ(I))	0.0554, 0.1535	0.0876, 0.2399	0.0510, 0.0936
$R_1{}^a$, $wR_2{}^b$(all data)	0.0682, 0.1643	0.1075, 0.2589	0.0844, 0.1103

$R_1{}^a = \Sigma||F_o| - |F_c||/\Sigma F_o|$. $wR_2{}^b = [\Sigma w(F_o{}^2 - F_c{}^2)^2/\Sigma w(F_o{}^2)^2]^{1/2}$

complexes	**4**	**5**
molecular formula	$C_{169}H_{132}Cl_4Dy_4N_{12}O_{12}$	$C_{47}H_{38}ClDyN_4O_3P$
formular weight	3375.59	936.74
crystal system	Triclinic	Monoclinic
space group	*P*-1	$P2_1/c$
a, Å	11.2499(16)	12.1506(3)
b, Å	18.894(2)	10.3478(3)
c, Å	36.404(5)	33.4047(8)
a, deg	83.682(4)	90
β, deg	84.689(5)	98.1990(10)
γ, deg	78.406(5)	90
V, Å^3	7514.3(17)	4157.11(19)
Z	2	4
ρ_{calcd},g cm^{-3}	1.492	1.497
T / K	273.15	193
μ, mm^{-1}	2.123	10.938
θ, deg	2.822 to 26.000	2.673 to 68.410
F(000)	3374	1884
index ranges	−13 ≤ h ≤ 13 −23 ≤ k ≤23 −44≤ l ≤ 44	−14 ≤ h ≤ 14 −12 ≤ k ≤12 −29≤ l ≤ 40
data/restraints/parameters	28941/547/1894	7591 / 146 / 558
GOF (F^2)	1.062	1.053
$R_1{}^a$,$wR_2{}^b$ (I>2σ(I))	0.0548, 0.0876	0.0369, 0.0968
$R_1{}^a$, $wR_2{}^b$(all data)	0.0916, 0.0947	0.0442,0.1010

$R_1{}^a = \Sigma||F_o| - |F_c||/\Sigma F_o|$. $wR_2{}^b = [\Sigma w(F_o{}^2 - F_c{}^2)^2/\Sigma w(F_o{}^2)^2]^{1/2}$

Table S2 Selected bond lengths (Å) and angles (°) for complex **1**.

Dy(1)-Cl(1)	2.627(2)	Dy(1)-N(1)	2.480(5)
Dy(1)-N(3A)	2.513(4)	Dy(1)-O(1A)	2.339(4)
Dy(1)-O(1)	2.305(4)	Dy(1)-O(2)	2.172(4)
Dy(1)-O(3)	2.234(5)	Dy(1)-Dy(1A)	3.866(5)

N(1)-Dy(1)-Cl(1)	93.71(14)	N(1)-Dy(1)-N(3A)	162.20(15)
N(3A)-Dy(1)-Cl(1)	89.05(12)	O(1A)-Dy(1)-Cl(1)	93.86(13)
O(1)-Dy(1)-Cl(1)	94.95(14)	O(1)-Dy(1)-N(1)	64.80(13)
O(1A)-Dy(1)-N(1)	131.93(14)	O(1)-Dy(1)-N(3A)	132.51(13)
O(1A)-Dy(1)-N(3A)	65.24(14)	O(1)-Dy(1)-O(1A)	67.28(15)
O(2)-Dy(1)-Cl(1)	91.61(14)	O(2)-Dy(1)-N(1)	74.89(14)
O(2)-Dy(1)-N(3A)	87.47(14)	O(2)-Dy(1)-O(1)	139.46(13)
O(2)-Dy(1)-O(1A)	152.01(14)	O(2)-Dy(1)-O(3)	87.44(19)
O(3)-Dy(1)-Cl(1)	176.63(14)	O(3)-Dy(1)-N(1)	89.18(18)
O(3)-Dy(1)-N(3A)	87.67(17)	O(3)-Dy(1)-O(1A)	85.49(18)
O(3)-Dy(1)-O(1)	87.86(18)	Dy(1)-O(1)-Dy(1A)	112.72(15)

Symmetry transformations used to generate equivalent atoms: A -x+1,-y+1,-z+2

Table S3 Selected bond lengths (Å) and angles (°) for complex **2**.

Dy(1)-Cl(1)	2.636(3)	Dy(1)-N(1)	2.474(8)
Dy(1)-N(3A)	2.507(8)	Dy(1)-O(1)	2.302(6)
Dy(1)-O(1A)	2.350(6)	Dy(1)-O(2)	2.170(7)
Dy(1)-O(3)	2.272(7)	Dy(1)-Dy(1A)	3.890(8)
N(1)-Dy(1)-Cl(1)	95.4(2)	N(1)-Dy(1)-N(3A)	163.1(3)
N(3A)-Dy(1)-Cl(1)	86.6(2)	O(1)-Dy(1)-Cl(1)	96.85(17)
O(1A)-Dy(1)-Cl(1)	91.35(17)	O(1A)-Dy(1)-N(1)	131.1(2)
O(1)-Dy(1)-N(1)	64.6(2)	O(1A)-Dy(1)-N(3A)	65.5(2)
O(1)-Dy(1)-N(3A)	131.9(2)	O(1)-Dy(1)-O(1A)	66.5(2)
O(2)-Dy(1)-Cl(1)	90.3(2)	O(2)-Dy(1)-N(1)	74.8(3)
O(2)-Dy(1)-N(3A)	88.4(3)	O(2)-Dy(1)-O(1A)	153.6(3)
O(2)-Dy(1)-O(1)	139.3(2)	O(2)-Dy(1)-O(3)	86.4(3)
O(3)-Dy(1)-Cl(1)	171.7(2)	O(3)-Dy(1)-N(1)	91.1(3)
O(3)-Dy(1)-N(3A)	85.7(3)	O(3)-Dy(1)-O(1)	90.5(3)
O(3)-Dy(1)-O(1A)	88.2(3)	Dy(1)-O(1)-Dy(1A)	113.5(2)

Symmetry transformations used to generate equivalent atoms: A -x+1,-y+1,-z+2

Table S4 Selected bond lengths (Å) and angles (°) for complex **3**.

Dy(1)-Cl(1)	2.619(1)	Dy(1)-O(1)	2.298(3)
Dy(1)-O(1A)	2.338(3)	Dy(1)-O(2)	2.181(3)
Dy(1)-O(3)	2.259(3)	Dy(1)-N(1A)	2.524(4)
Dy(1)-N(3)	2.475(4)	Dy(1)-Dy(1A)	3.868(4)
O(1)-Dy(1)-Cl(1)	92.87(9)	O(1)-Dy(1)-O(1A)	66.86(12)
O(A1)-Dy(1)-N(1A)	65.44(11)	O(1)-Dy(1)-N(1A)	132.16(11)
O(1A)-Dy(1)-N(3)	131.66(11)	O(1)-Dy(1)-N(3)	65.06(11)

O(1A)-Dy(1)-Cl(1)	88.67(9)	O(2)-Dy(1)-Cl(1)	90.73(10)
O(2)-Dy(1)-O(1A)	153.70(11)	O(2)-Dy(1)-O(1)	139.41(11)
O(2)-Dy(1)-O(3)	88.65(12)	O(2)-Dy(1)-N(1A)	88.27(12)
O(2)-Dy(1)-N(3)	74.60(12)	O(3)-Dy(1)-N(3)	96.51(12)
O(3)-Dy(1)-Cl(1)	174.15(9)	O(3)-Dy(1)-O(1)	91.38(11)
O(3)-Dy(1)-O(1A)	89.31(11)	O(3)-Dy(1)-N(1A)	84.70(12)
N(1A)-Dy(1)-Cl(1)	89.48(9)	N(3)-Dy(1)-N(1A)	162.77(12)
N(3)-Dy(1)-Cl(1)	88.93(10)	Dy(1)-O(1)-Dy(1A)	113.14(12)

Symmetry transformations used to generate equivalent atoms: A -x+1, -y+1,-z+1

Table S5 Selected bond lengths (Å) and angles (°) for complex **4**.

Dy(1)-Cl(2)	2.578(2)	Dy(1)-O(1)	2.155(4)
Dy(1)-O(2)	2.297(4)	Dy(1)-O(3)	2.335(4)
Dy(1)-N(1)	2.468(5)	Dy(1)-N(6)	2.521(5)
Dy(1)-O(12)	2.373(4)	Dy(2)-Cl(1)	2.655(2)
Dy(2)-O(2)	2.350(3)	Dy(2)-O(3)	2.303(3)
Dy(2)-O(4)	2.164(4)	Dy(2)-O(9)	2.277(4)
Dy(2)-N(3)	2.527(5)	Dy(2)-N(4)	2.450(4)
Dy(3)-Cl(3)	2.660(2)	Dy(3)-O(5)	2.175(4)
Dy(3)-O(6)	2.315(4)	Dy(3)-O(7)	2.327(4)
Dy(3)-O(11)	2.272(5)	Dy(3)-N(7)	2.454(5)
Dy(3)-N(10)	2.519(5)	Dy(4)-Cl(4)	2.571(2)
Dy(4)-O(6)	2.328(4)	Dy(4)-O(7)	2.303(4)
Dy(4)-O(8)	2.167(4)	Dy(4)-O(10)	2.405(5)
Dy(4)-N(9)	2.535(5)	Dy(4)-N(12)	2.467(5)
O(1)-Dy(1)-Cl(2)	93.49(12)	O(1)-Dy(1)-O(2)	138.37(13)
O(1)-Dy(1)-O(3)	149.55(14)	O(1)-Dy(1)-N(1)	74.37(15)
O(1)-Dy(1)-N(6)	87.35(14)	O(1)-Dy(1)-O(12)	86.24(16)
O(2)-Dy(1)-Cl(2)	102.34(11)	O(2)-Dy(1)-O(3)	66.78(12)
O(2)-Dy(1)-N(1)	64.48(14)	O(2)-Dy(1)-N(6)	131.75(13)
O(2)-Dy(1)-O(12)	84.60(15)	O(3)-Dy(1)-Cl(2)	96.44(10)
O(3)-Dy(1)-N(1)	129.84(14)	O(3)-Dy(1)-N(6)	65.02(13)
O(3)-Dy(1)-O(12)	78.88(14)	N(1)-Dy(1)-Cl(2)	104.59(12)
N(1)-Dy(1)-N(6)	159.63(15)	N(6)-Dy(1)-Cl(2)	85.10(12)
O(12)-Dy(1)-Cl(2)	169.47(13)	O(12)-Dy(1)-N(1)	85.50(17)
O(12)-Dy(1)-N(6)	84.37(17)	O(2)-Dy(2)-Cl(1)	85.82(10)
O(2)-Dy(2)-N(3)	65.23(13)	O(2)-Dy(2)-N(4)	131.34(13)
O(3)-Dy(2)-Cl(1)	87.29(10)	O(3)-Dy(2)-O(2)	66.44(12)
O(3)-Dy(2)-N(3)	131.63(14)	O(3)-Dy(2)-N(4)	65.06(14)

O(4)-Dy(2)-Cl(1)	98.26(12)	O(4)-Dy(2)-O(2)	152.45(14)
O(4)-Dy(2)-O(3)	140.67(13)	O(4)-Dy(2)-O(9)	90.07(16)
O(4)-Dy(2)-N(3)	87.38(15)	O(4)-Dy(2)-N(4)	75.64(14)
O(9)-Dy(2)-Cl(1)	171.47(11)	O(9)-Dy(2)-O(2)	85.94(14)
O(9)-Dy(2)-O(3)	87.42(14)	O(9)-Dy(2)-N(3)	87.35(15)
O(9)-Dy(2)-N(4)	88.24(15)	N(3)-Dy(2)-Cl(1)	91.17(12)
N(4)-Dy(2)-Cl(1)	95.57(12)	N(4)-Dy(2)-N(3)	162.45(15)
O(5)-Dy(3)-Cl(3)	96.71(13)	O(5)-Dy(3)-O(6)	140.40(14)
O(5)-Dy(3)-O(7)	152.93(15)	O(5)-Dy(3)-O(11)	88.90(18)
O(5)-Dy(3)-N(7)	75.63(15)	O(5)-Dy(3)-N(10)	86.96(16)
O(6)-Dy(3)-Cl(3)	88.44(12)	O(6)-Dy(3)-O(7)	66.52(14)
O(6)-Dy(3)-N(7)	64.77(14)	O(6)-Dy(3)-N(10)	132.33(15)
O(7)-Dy(3)-Cl(3)	84.86(12)	O(7)-Dy(3)-N(7)	131.20(15)
O(7)-Dy(3)-N(10)	65.97(15)	O(11)-Dy(3)-Cl(3)	172.69(13)
O(11)-Dy(3)-O(6)	90.21(16)	O(11)-Dy(3)-O(7)	88.02(17)
O(11)-Dy(3)-N(7)	89.44(17)	O(11)-Dy(3)-N(10)	84.46(17)
N(7)-Dy(3)-Cl(3)	96.47(13)	N(7)-Dy(3)-N(10)	161.67(16)
N(10)-Dy(3)-Cl(3)	91.14(13)	O(6)-Dy(4)-Cl(4)	95.37(12)
O(6)-Dy(4)-O(10)	78.56(16)	O(6)-Dy(4)-N(9)	65.43(15)
O(6)-Dy(4)-N(12)	130.30(15)	O(7)-Dy(4)-Cl(4)	96.00(13)
O(7)-Dy(4)-O(6)	66.69(13)	O(7)-Dy(4)-O(10)	84.77(17)
O(7)-Dy(4)-N(9)	132.09(15)	O(7)-Dy(4)-N(12)	64.72(15)
O(8)-Dy(4)-Cl(4)	96.61(16)	O(8)-Dy(4)-O(6)	149.62(16)
O(8)-Dy(4)-O(7)	139.01(15)	O(8)-Dy(4)-O(10)	87.2(2)
O(8)-Dy(4)-N(9)	86.71(16)	O(8)-Dy(4)-N(12)	74.81(16)
O(10)-Dy(4)-Cl(4)	173.05(13)	O(10)-Dy(4)-N(9)	84.33(18)
O(10)-Dy(4)-N(12)	87.29(19)	N(9)-Dy(4)-Cl(4)	90.09(14)
N(12)-Dy(4)-Cl(4)	99.30(15)	N(12)-Dy(4)-N(9)	160.05(17)
Dy(1)-O(2)-Dy(2)	113.00(14)	Dy(2)-O(3)-Dy(1)	113.38(15)
Dy(3)-O(6)-Dy(4)	113.03(15)	Dy(4)-O(7)-Dy(3)	113.51(16)

Table S6 Selected bond lengths (Å) and angles (°) for complex **5**.

Dy(1)-N(1)	2.459(3)	Dy(1)-N(3A)	2.536(3)
Dy(1)-O(1A)	2.337(2)	Dy(1)-O(1)	2.321(2)
Dy(1)-O(2)	2.187(2)	Dy(1)-O(3)	2.307(2)
Dy(1)-Cl(1)	2.627(1)	Dy(1)-Dy(1A)	3.902(4)
N(1)-Dy(1)-N(3A)	163.31(10)	N(1)-Dy(1)-Cl(1)	91.35(8)
N(3A)-Dy(1)-Cl(1)	91.52(7)	O(1A)-Dy(1)-N(1)	130.46(9)

O(1)-Dy(1)-N(1)	64.31(9)	O(1)-Dy(1)-N(3A)	131.89(9)
O(1A)-Dy(1)-N(3A)	65.96(9)	O(1)-Dy(1)-O(1A)	66.16(10)
O(1A)-Dy(1)-Cl(1)	90.33(7)	O(1)-Dy(1)-Cl(1)	93.22(7)
O(2)-Dy(1)-N(1)	74.57(10)	O(2)-Dy(1)-N(3A)	88.80(9)
O(2)-Dy(1)-O(1A)	154.43(9)	O(2)-Dy(1)-O(1)	138.27(9)
O(2)-Dy(1)-O(3)	85.13(10)	O(2)-Dy(1)-Cl(1)	94.61(7)
O(3)-Dy(1)-N(1)	99.66(11)	O(3)-Dy(1)-N(3A)	76.96(10)
O(3)-Dy(1)-O(1A)	85.13(9)	O(3)-Dy(1)-O(1)	94.61(9)
O(3)-Dy(1)-Cl(1)	168.47(8)	Dy(1)-O(1)-Dy(1A)	113.84(10)

Symmetry transformations used to generate equivalent atoms: A -x+1,-y+1,-z+1

Table S7 Continuous Shape Measures (CShMs) of the coordination geometry for Dy^{III} ion in all complexes. Below is the symmetry and description for each polyhedron.

Complexes	Atoms	PBPY-7 (D_{5h})	COC-7 (C_{3v})	CTPR-7 (C_{2v})	JPBPY-7 (D_{5h})
1	Dy1	**1.288**	7.571	6.224	5.448
2	Dy1	**1.448**	7.453	5.985	5.736
3	Dy1	**1.236**	6.896	5.568	5.440
4	Dy1	**1.839**	6.984	6.247	6.352
	Dy2	**1.127**	7.999	6.392	5.529
	Dy3	**1.200**	7.722	6.045	5.620
	Dy4	**1.373**	7.240	6.222	6.062
5	Dy1	**1.704**	7.313	5.643	5.979

PBPY-7 = Pentagonal bipyramid

COC-7 = Capped octahedron

CTPR-7 = Capped trigonal prism

JPBPY-7 = Johnson pentagonal bipyramid J13

Table S8 Magnetic relaxation parameters obtained by fitting the plot of $\ln\tau \sim T^{-1}$.

Complex	U_{eff} / K	τ_0 / s	C /$s^{-1}\cdot K^{-n}$	n	τ_{QTM} / s	adjusted R^2
1	45.76	2.16×10^{-5}	0.34	3.56	0.0096	0.99994
2	44.49	3.19×10^{-5}	2.19	2.26	0.0159	0.99985
3	66.49	5.56×10^{-6}	1.34	2.80	0.0338	0.99984
4	70.00	3.73×10^{-6}	0.52	2.89	0.1018	0.99956
5	63.13	1.53×10^{-5}	0.08	3.71	0.1329	0.99998

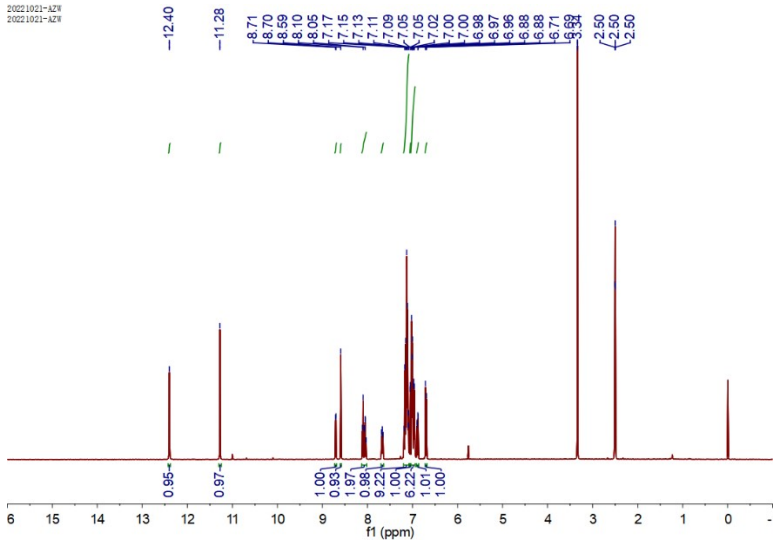

Fig. S1 [1]HNMR spectra of the H_2TPE-pc ligand.

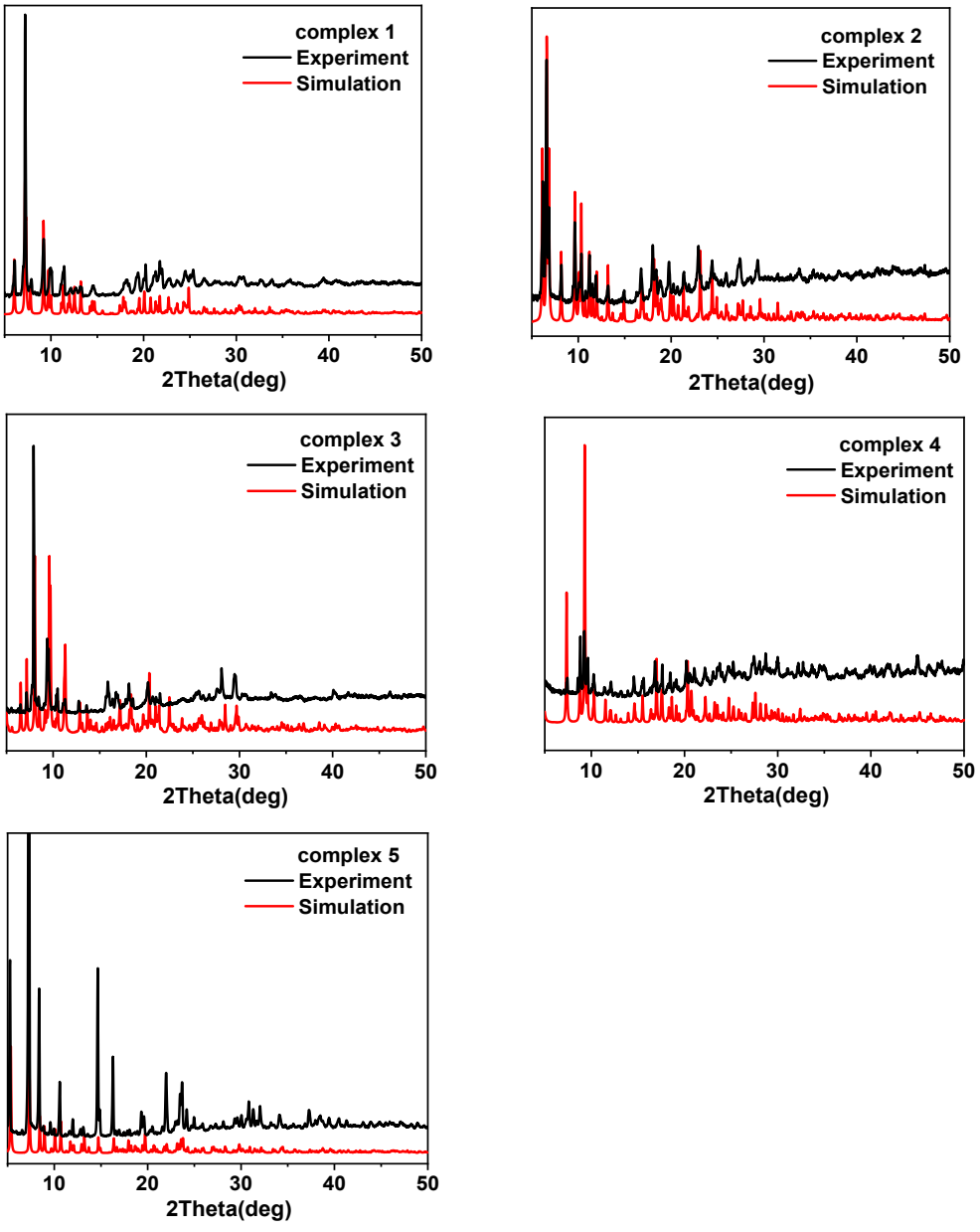

Fig. S2 PXRD patterns for all complexes.

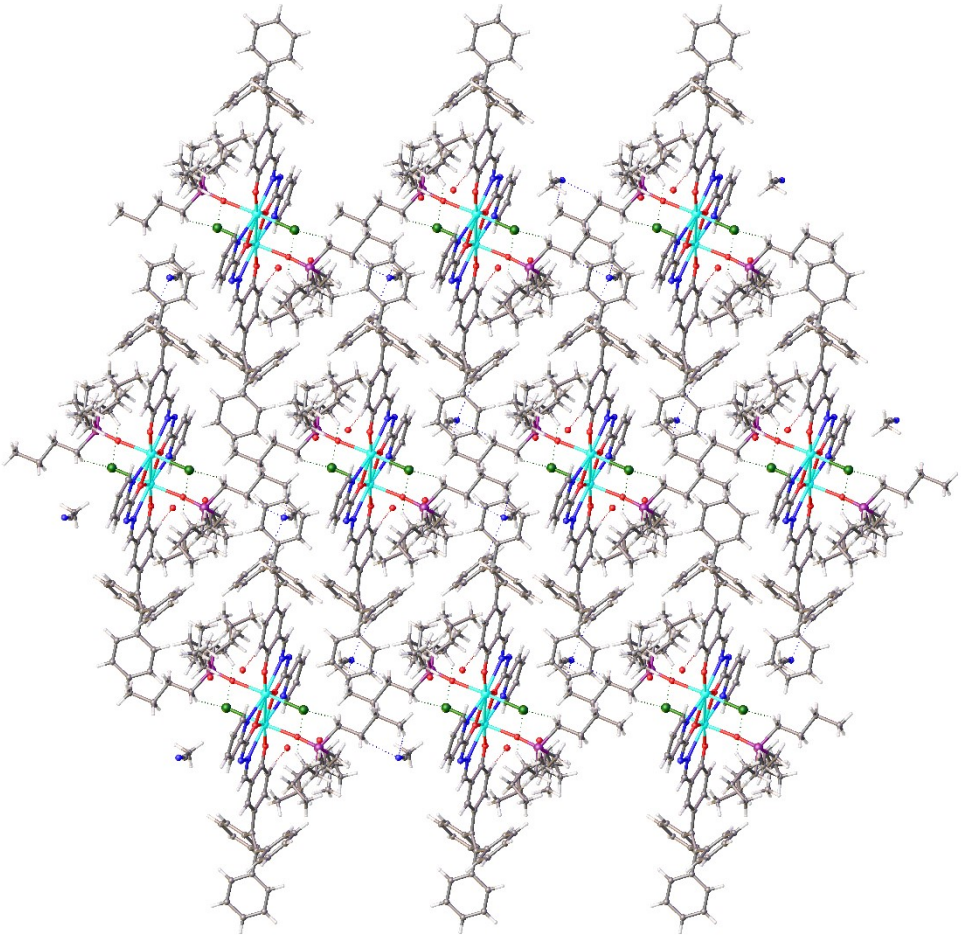

Fig. S3 A view showing 3D structure formed by weak C-H···Cl and C-H···N H-bond interactions and van der Waals forces in **1**.

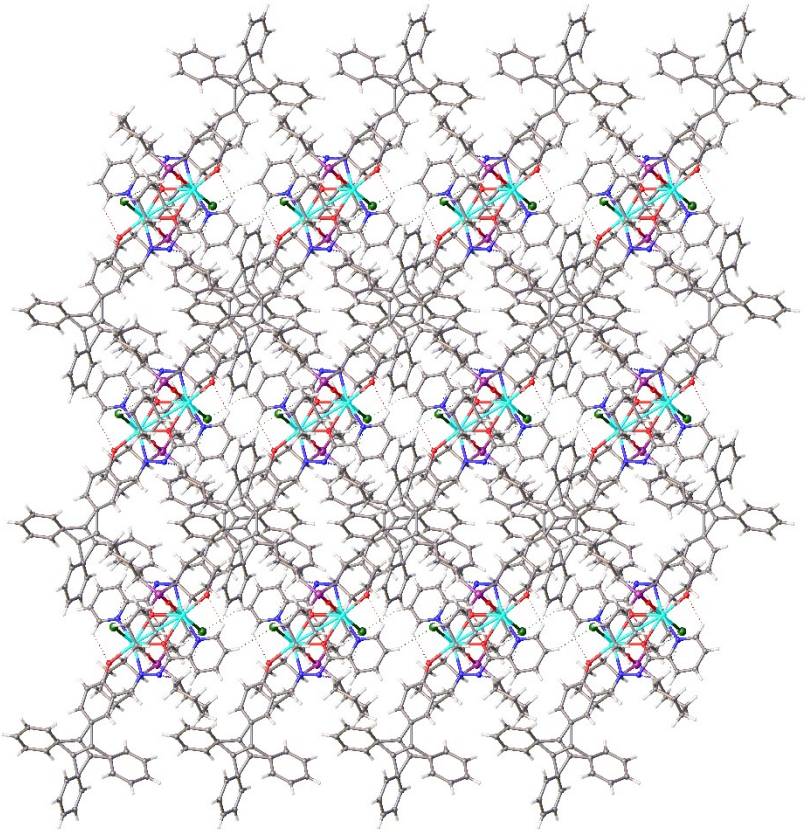

Fig. S4 A view showing 3D structure formed by weak C-H···O and C-H···Cl H-bond interactions and van der Waals forces in **2**.

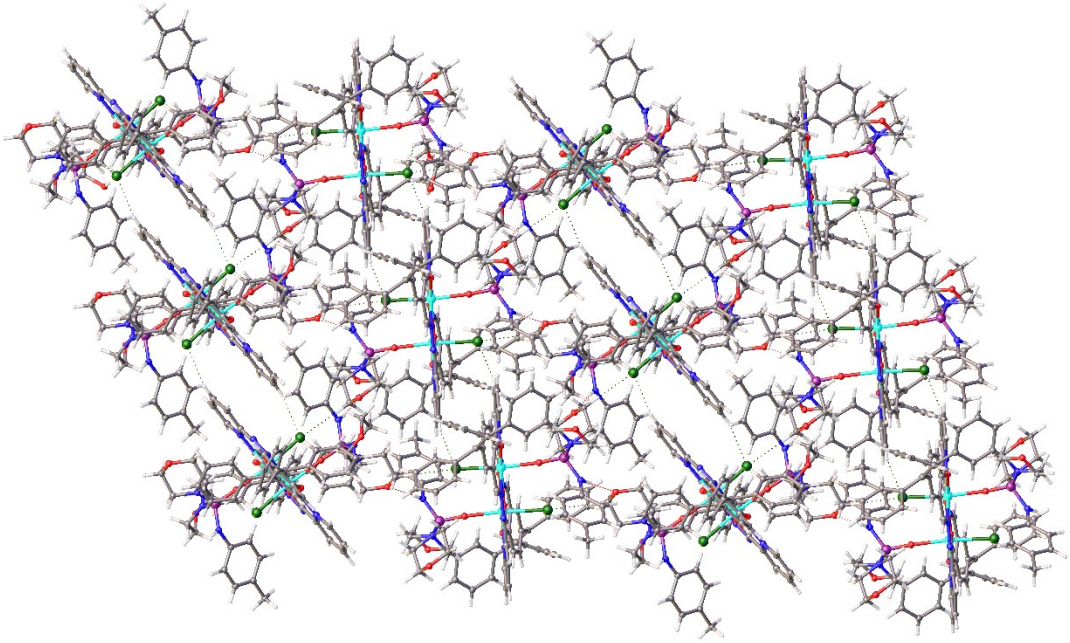

Fig. S5 A view showing 3D structure formed by weak C-H···Cl, N-H···O and π···π interactions in **3**.

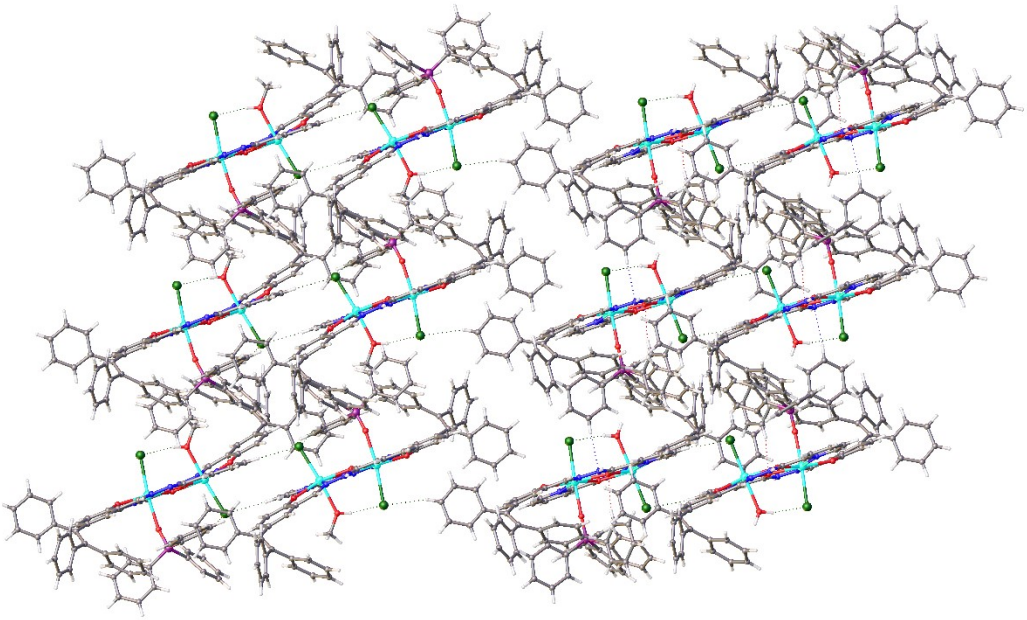

Fig. S6 A view showing 3D structure formed by weak C-H···Cl, C-H···N, O-H···Cl interactions in **4**.

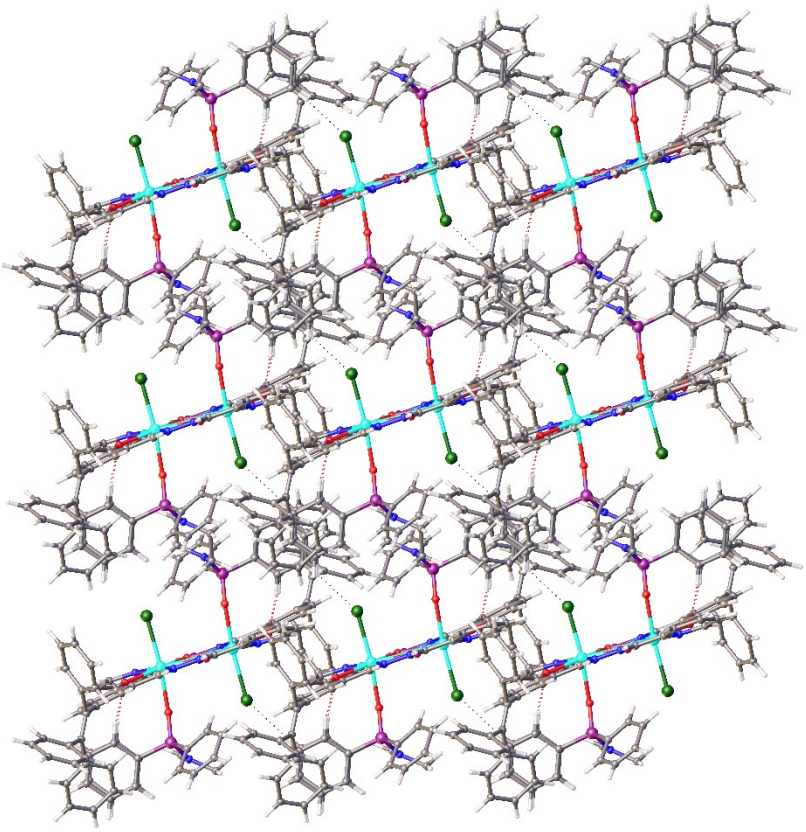

Fig. S7 A view showing 3D structure formed by weak C-H···Cl, C-H···O and π···π interactions in **5**.

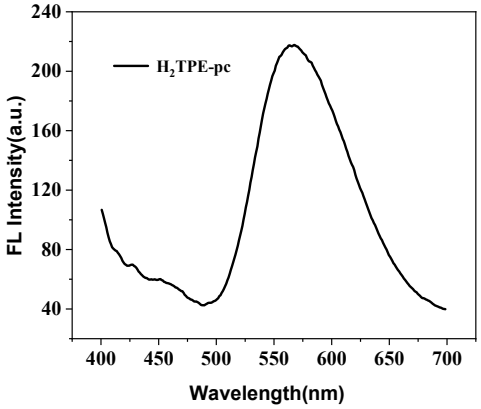

Fig. S8 The solid-state emission spectra of the H_2TPE-pc ligand at room temperature.

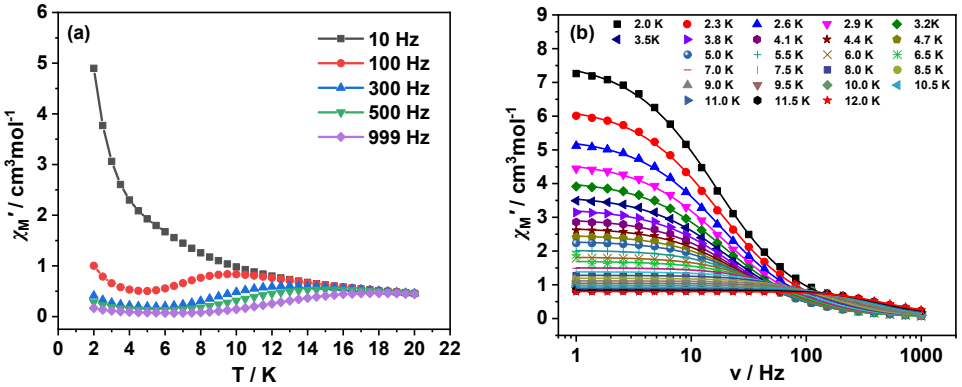

Fig. S9 Temperature(a) and frequency (b) dependence of the in-of-phase (χ') ac susceptibility signals for **1** under a zero-dc field. In figure (a), the solid lines are a guide for the eye. In figure (b), the solid lines are the best fit using the Debye model.

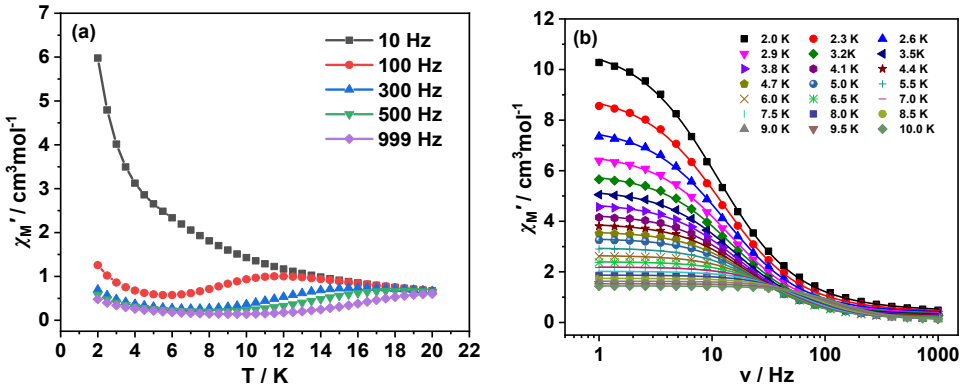

Fig. S10 Temperature(a) and frequency (b) dependence of the in-of-phase (χ') ac susceptibility signals for **2** under a zero-dc field. In figure (a), the solid lines are a guide for the eye. In figure (b), the solid lines are the best fit using the Debye model.

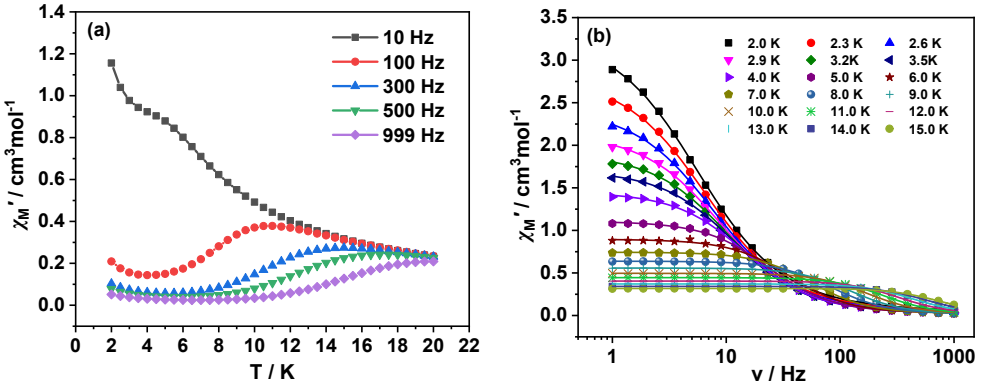

Fig. S11 Temperature(a) and frequency (b) dependence of the in-of-phase (χ') ac susceptibility signals for **3** under a zero-dc field. In figure (a), the solid lines are a guide for the eye. In figure (b), the solid lines are the best fit using the Debye model.

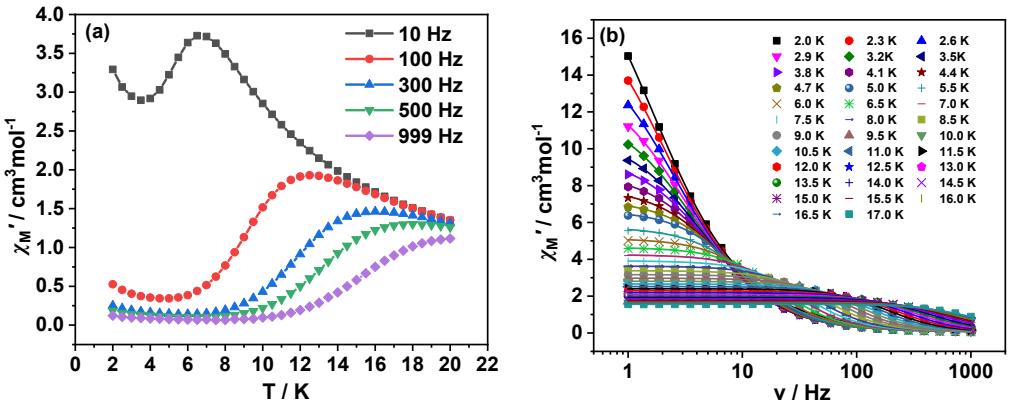

Fig. S12 Temperature(a) and frequency (b) dependence of the in-of-phase (χ') ac susceptibility signals for **4** under a zero-dc field. In figure (a), the solid lines are a guide for the eye. In figure (b), the solid lines are the best fit using the Debye model.

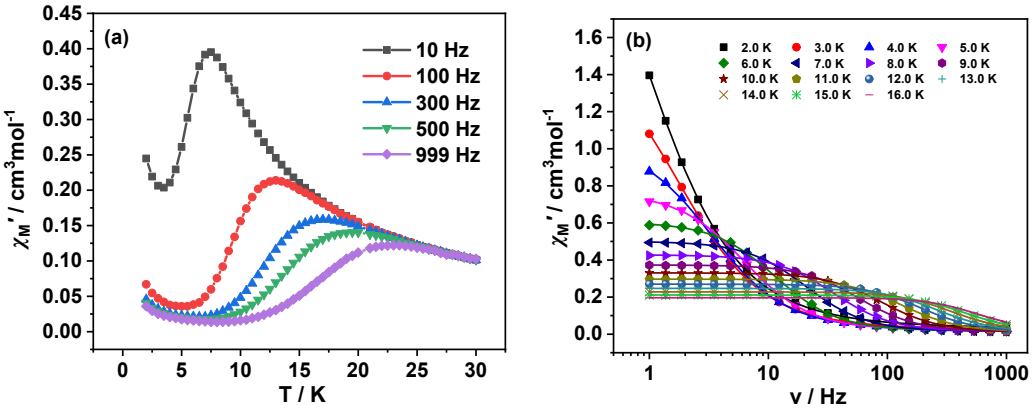

Fig. S13 Temperature(a) and frequency (b) dependence of the in-of-phase (χ') ac susceptibility signals for **5** under a zero-dc field. In figure (a), the solid lines are a guide for the eye. In figure (b), the solid lines are the best fit using the Debye model.

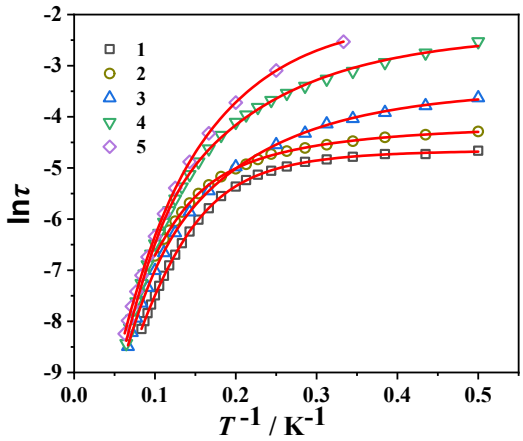

Fig. S14 Relaxation data plotted as ln(τ) vs. T^{-1} for **1**-**5**. The red solid lines represent the best fits of experimental data based on Orbach, Raman and QTM processes.

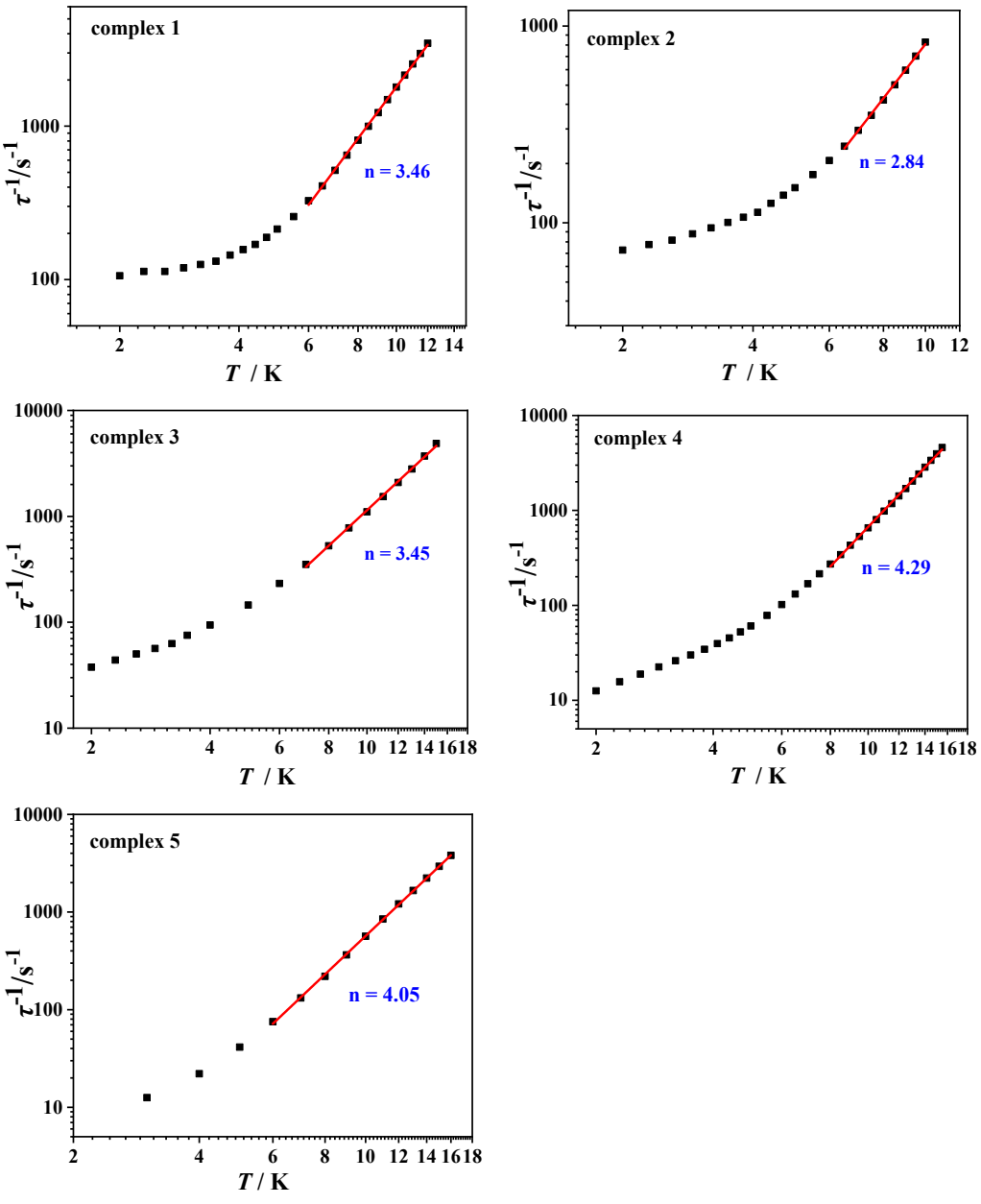

Fig. S15 Temperature-dependent relaxation times of **1-5** (log-log scale) under zero dc field. The lines were fitted to the equation of $\tau^{-1} = T^{n}$ to give n values.

Computational details

For binuclear complexes **1**–**3** and **5**, we only need to calculate one individual Dy^{III} fragment (**1_Dy1**, **2_Dy1**, **3_Dy1** and **5_Dy1**) respectively due to the centrosymmetric structure. But for complex **4**, which is also binucleated, we need to consider two molecular structures (**4-1**, **4-2**), each of which is not centrally symmetric, so four Dy^{III} fragments (**4_Dy1**, **4_Dy2**, **4_Dy3** and **4_Dy4)** need to be calculated (see Figure S15). Complete-active-space self-consistent field (CASSCF) calculations on individual Dy^{III} fragments have been carried out with the OpenMolcas[S1] program package. Each of individual Dy^{III} fragments in complexes was calculated keeping the experimentally determined structures of the corresponding compounds while replacing the other Dy^{III} ions with diamagnetic Lu^{III}.

The basis sets for all atoms are atomic natural orbitals from the ANO-RCC library: ANO-RCC-VTZP for Dy^{III}; VTZ for close N and O; VDZ for distant atoms. The calculations employed the second order Douglas-Kroll-Hess Hamiltonian, where scalar relativistic contractions were taken into account in the basis set and the spin-orbit couplings were handled separately in the restricted active space state interaction (RASSI-SO) procedure.[S2,S3] For each individual Dy^{III} fragment, active electrons in 7 active orbitals include all *f* electrons (CAS(9 in 7 for Dy^{III})) in the CASSCF calculation. To exclude all the doubts, we calculated all the roots in the active space. We have mixed the maximum number of spin-free state which was possible with our hardware (all from 21 sextets, 128 from 224 quadruplets, 130 from 490 doublets) for each fragment. The SINGLE_ANISO[S4–S6] program was used to obtain the energy levels, ***g*** tensors, magnetic axes, *et al.* based on the above CASSCF/RASSI-SO calculations.

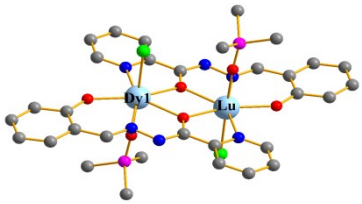

1_Dy1

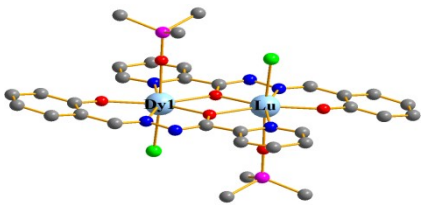

2_Dy1

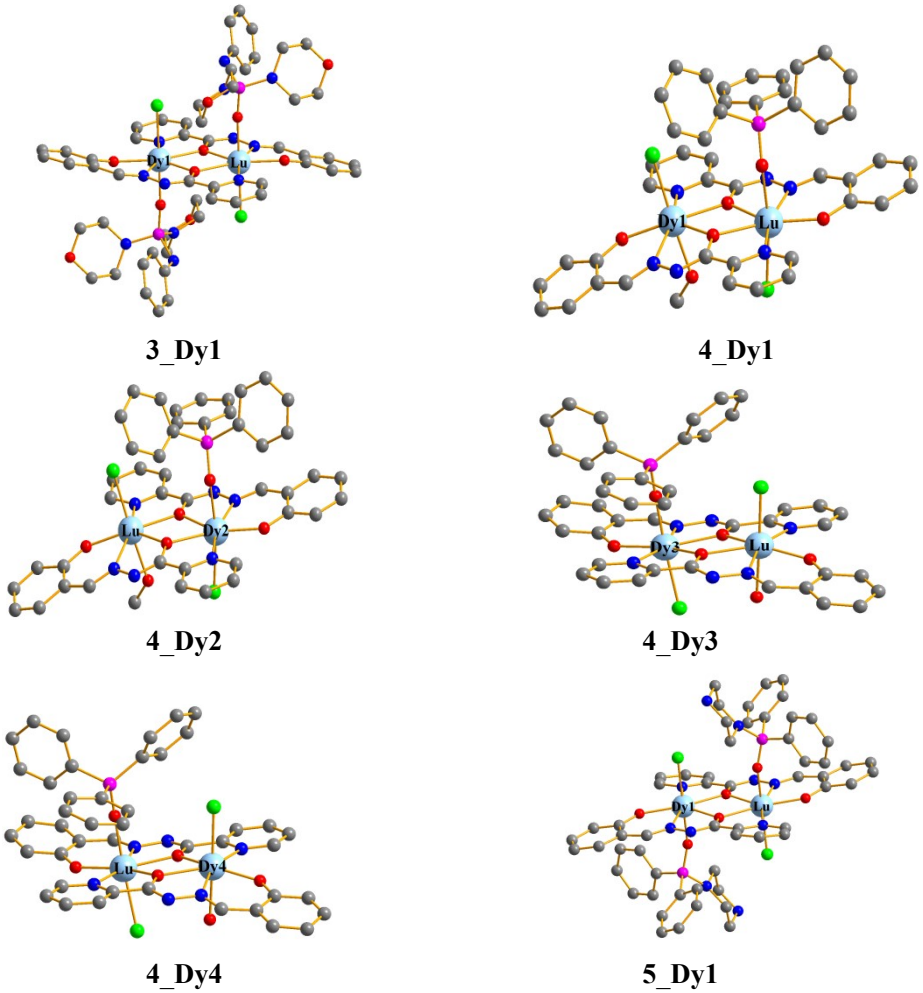

Fig. S16 Calculated model structures of individual Dy^{III} fragments of complexes **1**–**5**; H atoms are omitted for clarify.

Table S9. Calculated energy levels (cm^{-1}), $\boldsymbol{g}$ (g_x, g_y, g_z) tensors and predominant m_J values of the lowest eight Kramers doublets (KDs) of individual Dy^{III} fragments for complexes **1**–**5** using CASSCF/RASSI-SO with the OpenMolcas.

KDs	**1_Dy1**			**2_Dy1**			**3_Dy1**		
	E	***g***	m_J	*E*	***g***	m_J	*E*	***g***	m_J
1	0.0	0.001 0.008 19.668	±15/2	0.0	0.001 0.005 19.697	±15/2	0.0	0.007 0.014 19.681	±15/2
2	194.3	0.267 0.342 16.970	±13/2	200.9	0.176 0.196 17.142	±13/2	195.3	0.180 0.239 17.037	±13/2
3	298.8	1.118 1.408 18.329	±1/2	350.4	2.068 3.962 15.422	±3/2	317.3	1.292 1.705 17.988	±1/2
4	376.0	2.962 5.713 10.229	±11/2	394.8	8.184 6.308 0.213	±11/2	381.8	2.046 5.641 10.160	±11/2
5	471.8	9.617 5.363 0.661	±9/2	479.2	0.659 4.913 12.460	±5/2	472.0	0.295 4.804 11.568	±9/2

6	494.8	1.546 2.548 12.472	±7/2	527.9	4.231 5.135 10.516	±7/2	508.1	2.605 3.525 12.813	±7/2
7	573.7	0.222 1.643 15.608	±3/2	593.4	0.529 0.787 16.283	±3/2	583.4	0.768 1.516 15.787	±3/2
8	619.4	0.964 1.439 17.749	±1/2	639.9	0.954 1.247 18.127	±1/2	627.6	1.027 1.897 17.503	±1/2
KDs	**4_Dy1**			**4_Dy2**			**4_Dy3**		
	E	***g***	m_J	*E*	***g***	m_J	*E*	***g***	m_J
1	0.0	0.008 0.015 19.600	±15/2	0.0	0.003 0.009 19.721	±15/2	0.0	0.003 0.009 19.699	±15/2
2	208.9	0.150 0.200 16.894	±13/2	205.9	0.203 0.219 17.166	±13/2	193.8	0.199 0.221 17.114	±13/2
3	391.6	3.420 5.488 10.530	±11/2	367.7	1.587 4.666 12.691	±11/2	353.7	1.069 3.533 12.843	±11/2
4	444.0	10.838 5.610 0.081	±1/2	404.9	8.000 6.781 0.864	±1/2	388.3	8.582 7.211 0.209	±1/2
5	482.9	2.040 2.852 14.371	±5/2	490.1	11.049 5.896 0.028	±5/2	458.7	0.796 5.703 11.409	±5/2
6	544.7	10.397 7.154 1.866	±9/2	543.6	3.719 3.849 11.341	±7/2	526.5	3.590 4.165 11.181	±7/2
7	583.1	1.950 2.231 13.552	±7/2	621.0	0.657 2.353 15.171	±3/2	590.4	0.785 2.498 15.892	±3/2
8	737.1	0.098 0.135 19.500	±1/2	657.2	1.178 3.010 16.722	±1/2	634.3	0.922 1.404 17.537	±7/2
KDs	**4_Dy4**			**5_Dy1**					
	E	***g***	m_J	*E*	***g***	m_J			
1	0.0	0.012 0.021 19.627	±15/2	0.0	0.005 0.011 19.674	±15/2			
2	215.1	0.209 0.276 16.879	±13/2	185.3	0.144 0.193 17.032	±13/2			

3	406.6	2.520 4.821 11.405	±11/2	316.8	0.846 1.307 17.339	±1/2			
4	477.6	9.662 7.426 0.883	±1/2	384.9	1.970 4.368 10.109	±11/2			
5	535.1	0.048 5.106 13.857	±5/2	471.4	1.395 4.521 13.031	±3/2			
6	582.7	3.840 5.770 9.475	±9/2	508.7	2.930 4.375 10.070	±7/2			
7	648.2	0.951 1.166 18.001	±5/2	560.1	0.622 2.122 13.432	±9/2			
8	709.2	0.274 0.433 19.245	±1/2	661.3	0.152 0.263 18.788	±7/2			

Table S10. Wave functions with definite projection of the total moment | m_J > for the lowest eight KDs of individual Dy^{III} fragments for complexes **1**–**5** using CASSCF/RASSI-SO with the OpenMolcas.

	E/cm^{-1}	wave functions
1_Dy1	0.0	94.7%|±15/2>
	194.3	86.2%|±13/2>+6.3%|±11/2>
	298.8	32.3%|±1/2>+27.8%|±3/2>+13.2%|±5/2>+10.4%|±11/2>+7.8%|±9/2>+7.8%|±7/2>
	376.0	55.1%|±11/2>+12.8%|±1/2>+10.8%|±9/2>+8.7%|±13/2>+5.7%|±7/2>
	471.8	25.8%|±9/2>+23%|±5/2>+22.2%|±3/2>+11.7%|±1/2>+10.2%|±11/2>
	632.3	47.2%|±7/2>+22.2%|±9/2>+19.3%|±5/2>+5.9%|±11/2>
	707.2	25.6%|±3/2>+23.2%|±5/2>+17.1%|±9/2>+13.1%|±7/2>+12%|±1/2>
	754.6	27.1%|±1/2>+21.5%|±7/2>+19.3%|±3/2>+18%|±5/2>+12.3%|±9/2>
2_Dy1	0.0	97.4%|±15/2>
	200.9	83.3%|±13/2>+8.3%|±11/2>
	350.4	27.2%|±3/2>+23.5%|±11/2>+23.2%|±1/2>+10.6%|±5/2>+8.8%|±9/2>
	394.8	37.5%|±11/2>+23.1%|±1/2>+12.9%|±7/2>+10.6%|±9/2>+9.6%|±13/2>
	479.2	30.5%|±5/2>+21.4%|±3/2>+19%|±9/2>+12.2%|±1/2>+7.9%|±11/2>
	527.9	44%|±7/2>+28%|±9/2>+12.3%|±5/2>+12.1%|±11/2>

	593.4	28.7%|±3/2>+26.3%|±5/2>+15.3%|±9/2>+12.1%|±7/2>+10.1%|±1/2>+7.1%|±11/2>
	639.9	28.8%|±1/2>+20.2%|±7/2>+18.7%|±3/2>+16.9%|±5/2>+13.2%|±9/2>
3_Dy1	0.0	97.1%|±15/2>
	195.3	85.1%|±13/2>+6.8%|±11/2>
	317.3	31.3%|±1/2>+28%|±3/2>+12.9%|±5/2>+12.3%|±11/2>+7.6%|±9/2>
	381.8	52.8%|±11/2>+13.8%|±1/2>+9.5%|±13/2>+9.1%|±9/2>+8.2%|±7/2>
	472.0	27.7%|±9/2>+25%|±5/2>+20.8%|±3/2>+11.7%|±1/2>+7.8%|±11/2>
	508.1	46.7%|±7/2>+20.4%|±9/2>+18.6%|±5/2>+8.1%|±11/2>
	583.4	27.2%|±3/2>+22.1%|±5/2>+19.5%|±9/2>+11.3%|±7/2>+10.2%|±1/2>
	627.6	28.7%|±1/2>+21.7%|±7/2>+18.8%|±3/2>+18.6%|±5/2>+11%|±9/2>
4_Dy1	0.0	95.6%|±15/2>
	208.9	84.6%|±13/2>+6.5%|±9/2>
	391.6	48.7%|±11/2>+20.8%|±3/2>+11.8%|±1/2>+5.4%|±7/2>+5.1%|±13/2>
	444.0	49.6%|±1/2>+17.6%|±9/2>+14%|±11/2>+5.7%|±7/2>+5.2%|±13/2>
	482.9	33.3%|±5/2>+29.4%|±3/2>+17%|±7/2>+7.9%|±11/2>+6.4%|±9/2>
	544.7	32.9%|±9/2>+20.4%|±7/2>+13.6%|±11/2>+13.3%|±5/2>+11.6%|±3/2>
	583.1	33.9%|±7/2>+24.9%|±5/2>+24.5%|±9/2>+10.3%|±3/2>
	737.1	27.7%|±1/2>+24.4%|±3/2>+20%|±5/2>+16.1%|±7/2>+9.1%|±9/2>
4_Dy2	0.0	97.9%|±15/2>
	205.9	82.2%|±13/2>+9%|±11/2>
	367.7	38.3%|±11/2>+22.5%|±3/2>+11.7%|±1/2>+11.5%|±9/2>+7.1%|±5/2>
	404.9	33.1%|±1/2>+21.4%|±11/2>+17%|±7/2>+9.9%|±9/2>+7.2%|±13/2>+6.2%|±3/2>
	490.1	29.9%|±5/2>+22%|±9/2>+21.1%|±3/2>+8.5%|±1/2>+8%|±11/2>+6.7%|±7/2>
	543.6	41.1%|±7/2>+22.8%|±9/2>+15%|±5/2>+12.4%|±11/2>
	621.0	34%|±3/2>+26.6%|±5/2>+14.3%|±9/2>+9.1%|±7/2>+8.3%|±11/2>
	657.2	32.8%|±1/2>+22.1%|±7/2>+14.7%|±5/2>+14.6%|±3/2>+14.2%|±9/2>
4_Dy3	0.0	97.4%|±15/2>
	193.8	82.3%|±13/2>+8.4%|±11/2>
	353.7	40%|±11/2>+24.2%|±3/2>+10.6%|±9/2>+10.3%|±1/2>+6.8%|±5/2>
	388.3	39.1%|±1/2>+18.8%|±7/2>+17.5%|±11/2>+9.5%|±9/2>+5.9%|±13/2>
	458.7	32.9%|±5/2>+22.1%|±3/2>+17.8%|±9/2>+9.8%|±11/2>+6.9%|±1/2>+5.8%|±7/2>
	526.5	39.1%|±7/2>+27.8%|±9/2>+13%|±11/2>+9.6%|±1/2>+8.4%|±5/2>
	590.4	37.7%|±3/2>+32.9%|±5/2>+10.7%|±1/2>+7.2%|±9/2>+5.5%|±11/2>
	634.3	27.5%|±7/2>+23.4%|±1/2>+21.5%|±9/2>+13.3%|±5/2>+9.9%|±3/2>
4_Dy4	0.0	96.1%|±15/2>
	215.1	85.7%|±13/2>+6.3%|±9/2>
	406.6	58.9%|±11/2>+13.8%|±3/2>+8.2%|±7/2>+6.5%|±13/2>+4.7%|±1/2>
	477.6	40.4%|±1/2>+27.9%|±9/2>+12.1%|±11/2>+5.7%|±7/2>+4.6%|±13/2>
	535.1	37%|±5/2>+32.5%|±3/2>+13.3%|±7/2>+9.2%|±1/2>

	582.7	41.1%|±9/2>+31.9%|±7/2>+13.1%|±11/2>+4.9%|±5/2>
	648.2	29.1%|±5/2>+22.3%|±3/2>+21.6%|±7/2>+13%|±1/2>+11.3%|±9/2>
	709.2	27.9%|±1/2>+23.6%|±3/2>+20.2%|±5/2>+17.8%|±7/2>+8.8%|±9/2>
5_Dy1	0.0	96.9%|±15/2>
	185.3	88.6%|±13/2>+5.6%|±11/2>
	316.8	28.3%|±1/2>+24.9%|±3/2>+17.1%|±11/2>+12.1%|±5/2>+9.7%|±9/2>
	384.9	53.3%|±11/2>+17.1%|±1/2>+9.4%|±9/2>+7.2%|±13/2>+6.3%|±7/2>
	471.4	26%|±3/2>+22.5%|±9/2>+21.9%|±5/2>+11%|±1/2>+10.1%|±7/2>
	508.7	27.7%|±7/2>+19%|±5/2>+18.8%|±1/2>+16.7%|±9/2>+10.7%|±3/2>
	560.1	25.3%|±9/2>+24.7%|±7/2>+22.7%|±5/2>+15.7%|±3/2>+6.1%|±11/2>
	661.3	23%|±7/2>+21.3%|±5/2>+19.6%|±1/2>+19.4%|±3/2>+13.4%|±9/2>

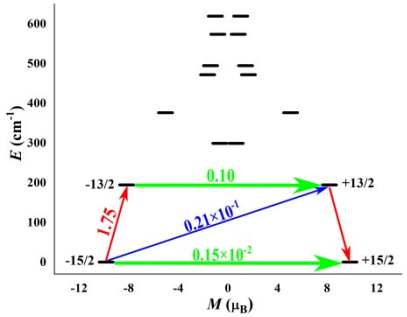

1_Dy1

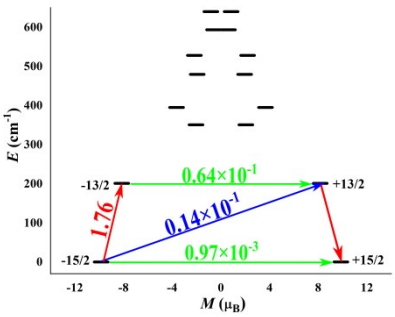

2_Dy1

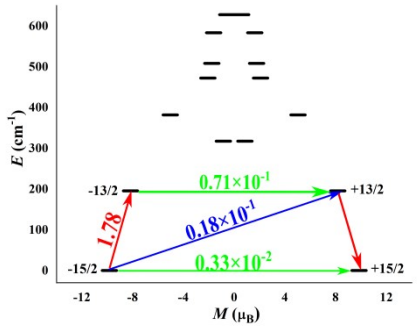

3_Dy1

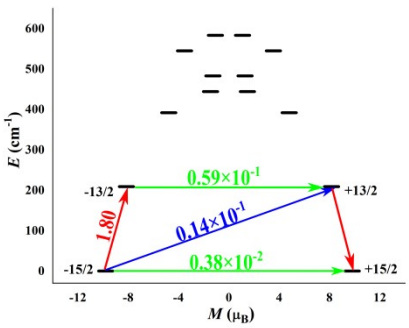

4_Dy1

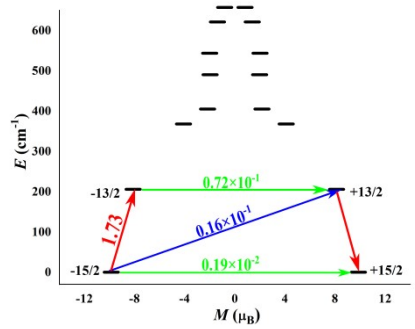

4_Dy2

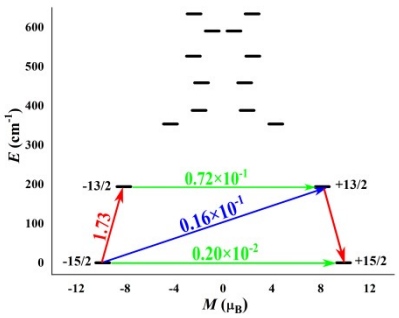

4_Dy3

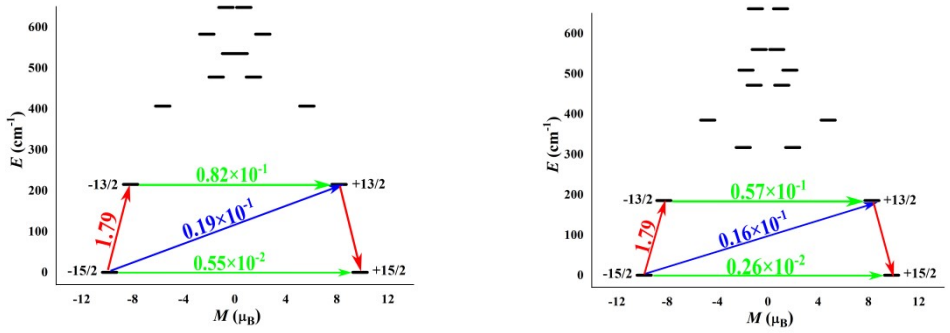

4_Dy4 **5_Dy1**

Fig. S17 Magnetization blocking barriers of individual Dy^{III} fragments for complexes **1**–**5**. The thick black lines represent the KDs of the individual Dy^{III} fragments as a function of their magnetic moment along the magnetic axis. The green lines correspond to diagonal matrix element of the transversal magnetic moment; the blue lines represent Orbach relaxation processes. The path shown by the red arrows represents the most probable path for magnetic relaxation in the corresponding compounds. The numbers at each arrow stand for the mean absolute value of the corresponding matrix element of transition magnetic moment.

To fit the exchange interactions between Dy^{III} ions in complexes **1**–**5**, we took two steps to obtain them. Firstly, we calculated individual Dy^{III} fragments using CASSCF/RASSI-SO to obtain the corresponding magnetic properties. Then, the exchange interaction between the magnetic centers was considered within the Lines model, [S7] while the account of the dipole-dipole magnetic coupling is treated exactly. The Lines model is effective and has been successfully used widely in the research field of *d* and *f*-elements single-molecule magnets. [S8, S9]

We only consider the interactions between the nearest neighbour Dy^{III} ions. Thus, for complexes **1**–**5**, there is only one type of $\tilde{J}$.

The Ising exchange Hamiltonian for **1**–**5** is:

$$\hat{H}_{exch} = -\tilde{J}\hat{S}_{Dy1}\hat{S}_{Dy2} \qquad \text{(S1)}$$

where $\tilde{J} = 25\cos\varphi J$, φ is the angle between the anisotropy axes on sites Dy1 and Dy2, and J is the Lines exchange coupling parameter. The $\hat{S}_{Dy} = 1/2$ is the ground pseudospin on the Dy^{III} site. The total $\tilde{J}_{total}$ is the parameter of the total magnetic interaction ($\tilde{J}_{total} = \tilde{J}_{dipolar} + \tilde{J}_{exchange}$) between magnetic center ions. The dipolar magnetic couplings can be calculated exactly, while the Lines exchange coupling constants were fitted through comparison of the computed and measured magnetic susceptibilities using the POLY_ANISO program.[S4–S6]

Table S11. Exchange energies E (cm^{-1}), the transversal magnetic moments Δ_t (cm^{-1}) and the main values of the g_z for the lowest two exchange doublets of complexes **1**–**5**.

	1			**2**		
exchange doublets	E	Δ_t	g_z	E	Δ_t	g_z
1	0.000000000000	3.066×10^{-7}	39.337	0.000000000000	4.676×10^{-8}	39.395
	0.000000336613			0.000000046761		
2	2.332671384909	3.541×10^{-7}	0.000	3.223884231561	5.634×10^{-8}	0.000
	2.332671738984			3.223884287897		
	3			**4-1**		
exchange doublets	E	Δ_t	g_z	E	Δ_t	g_z
1	0.000000000000	2.325×10^{-6}	39.362	0.000000000000	8.598×10^{-7}	39.106
	0.000002324782			0.000000859815		
2	0.309343811103	3.471×10^{-6}	0.000	1.454178112935	1.204×10^{-6}	4.115
	0.309347281803			1.454179316856		
	4-2			**5**		
exchange doublets	E	Δ_t	g_z	E	Δ_t	g_z
1	0.000000000000	9.563×10^{-7}	39.149	0.000000000000	3.505×10^{-7}	39.349
	0.000000956329			0.000000351528		
2	2.024876112109	1.373×10^{-6}	3.741	2.464844854685	5.342×10^{-7}	0.000
	2.024877485277			2.464845388853		

References:

S1 I. F. Galván, M. Vacher, A. Alavi, C. Angeli, F. Aquilante, J. Autschbach, J. J. Bao, S. I. Bokarev, N. A. Bogdanov, R. K. Carlson, L. F. Chibotaru, J. Creutzberg, N. Dattani, M. G. Delcey, S. S. Dong, A. Dreuw, L. Freitag, L. M. Frutos, L. Gagliardi, F. Gendron, A. Giussani, L. González, G. Grell, M. Y. Guo, C. E. Hoyer, M. Johansson, S. Keller, S. Knecht, G. Kovacevic, E. Källman, G. L. Manni, M. Lundberg, Y. J. Ma, S. Mai, J. P. Malhado, P. Å. Malmqvist, P. Marquetand, S. A. Mewes, J. Norell, M. Olivucci, M. Oppel, Q. M. Phung, K. Pierloot, F. Plasser, M. Reiher, A. M. Sand, I. Schapiro, P. Sharma, C. J. Stein, L. K. Sørensen, D. G. Truhlar, M. Ugandi, L. Ungur, A. Valentini, S. Vancoillie, V. Veryazov, O. Weser, T. A. Wesołowski, Per-Olof. Widmark, S. Wouters, A. Zech, J. P. Zobel, R. Lindh. OpenMolcas: From Source Code to Insight. *J. Chem. Theory Comput.* 2019, **15**, 5925–5964.

S2 P. Å. Malmqvist, B. O. Roos, B. Schimmelpfennig, The restricted active space (RAS) state interaction approach with spin–orbit coupling *Chem. Phys. Lett.,* 2002, **357***,* 230–240.

S3 B. A. Heß, C. M. Marian, U. Wahlgren, O. Gropen, A mean-field spin-orbit method applicable to correlated wavefunctions *Chem. Phys. Lett.,* 1996, **251***,* 365–371.

S4 L. F. Chibotaru, L. Ungur, A. Soncini, The Origin of Nonmagnetic Kramers Doublets in the Ground State of Dysprosium Triangles: Evidence for a Toroidal Magnetic Moment *Angew.*

Chem., Int. Ed. 2008, **47**, 4126–4129.

S5 L. Ungur, W. Van den Heuvel, L. F. Chibotaru, Ab initio investigation of the non-collinear magnetic structure and the lowest magnetic excitations in dysprosium triangles *New J. Chem.* 2009, **33**, 1224–1230.

S6 L. F. Chibotaru, L. Ungur, C. Aronica, H. Elmoll, G. Pilet, D. Luneau, Structure, Magnetism, and Theoretical Study of a Mixed-Valence $Co^{II}_3Co^{III}_4$ Heptanuclear Wheel: Lack of SMM Behavior despite Negative Magnetic Anisotropy *J. Am. Chem. Soc*. 2008, **130**, 12445–12455.

S7 M. E. Lines, Orbital Angular Momentum in the Theory of Paramagnetic Clusters *J. Chem. Phys*. 1971, **55**, 2977−2984.

S8 K. C. Mondal, A. Sundt, Y. H. Lan, G. E. Kostakis, O. Waldmann, L. Ungur, L. F. Chibotaru, C. E. Anson, A. K. Powell, Coexistence of Distinct Single-Ion and Exchange-Based Mechanisms for Blocking of Magnetization in a $Co^{II}_2Dy^{III}_2$ Single-Molecule Magnet *Angew. Chem., Int. Ed.* 2012, **51**, 7550−7554.

S9 S. K. Langley, D. P. Wielechowski, V. Vieru, N. F. Chilton, B. Moubaraki, B. F. Abrahams, L. F. Chibotaru, K. S. Murray, A $\{Cr^{III}_2Dy^{III}_2\}$ Single-Molecule Magnet: Enhancing the Blocking Temperature through 3d Magnetic Exchange *Angew. Chem., Int. Ed.* 2013, **52**, 12014–12019.